A novel target recognition revealed by calmodulin in complex with Ca^{2+}-calmodulin-dependent kinase kinase

Masanori Osawa[1,2], Hiroshi Tokumitsu[3], Mark B. Swindells[2–4], Hiroyuki Kurihara[1], Masaya Orita[1], Tadao Shibanuma[1], Toshio Furuya[3] and Mitsuhiko Ikura[5]

[1]Molecular Chemistry Research, Chemistry Laboratories, Institute for Drug Discovery Research, Yamanouchi Pharmaceutical Co., Ltd., Tsukuba 305-8585, Japan. [2]Center for Tsukuba Advanced Research Alliance and Institute of Applied Biochemistry, University of Tsukuba, Tsukuba 305-0006, Japan. [3]Helix Research Institute, Kisarazu 292-0812, Japan. [4]Current address: Inpharmatica, London W1P 2AX, UK. [5]Division of Molecular and Structural Biology, Ontario Cancer Institute and Department of Medical Biophysics, University of Toronto, Ontario M5G 2M9, Canada.

The structure of calcium-bound calmodulin (Ca^{2+}/CaM) complexed with a 26-residue peptide, corresponding to the CaM-binding domain of rat Ca^{2+}/CaM-dependent protein kinase kinase (CaMKK), has been determined by NMR spectroscopy. In this complex, the CaMKK peptide forms a fold comprising an α-helix and a hairpin-like loop whose C-terminus folds back on itself. The binding orientation of this CaMKK peptide by the two CaM domains is opposite to that observed in all other CaM–target complexes determined so far. The N- and C-terminal hydrophobic pockets of Ca^{2+}/CaM anchor Trp 444 and Phe 459 of the CaMKK peptide, respectively. This 14-residue separation between two key hydrophobic groups is also unique among previously determined CaM complexes. The present structure represents a new and distinct class of Ca^{2+}/CaM target recognition that may be shared by other Ca^{2+}/CaM-stimulated proteins.

Calmodulin (CaM)-dependent protein kinase kinase (CaMKK) is located at the top of a Ca^{2+}/CaM-dependent cascade that activates two serine/threonine kinases: CaM-kinase I (CaMKI) and CaM-kinase IV (CaMKIV)[1–5]. Upon activation by Ca^{2+}/CaM, CaMKK phosphorylates CaMKI and CaMKIV, and enhances their catalytic activities. CaMKI and CaMKIV themselves are also Ca^{2+}/CaM-dependent enzymes. This double modulation of the kinase activities by the calcium signal produces an amplification of Ca^{2+} sensitivity in cellular processes. In neurons, the CaMKK–CaMKIV signaling cascade activates the transcription of c-fos through phosphorylation of cAMP response element binding protein (CREB)[6–11], thereby modulating synaptic activity of specific intensity or duration[12]. In addition, Yano *et al.* recently provided evidence that CaMKK displays an anti-apoptotic effect, in response to modest elevation of intracellular Ca^{2+}, through phosphorylation and activation of protein kinase B (PKB)[13]. This observation suggests a direct linkage between the Ca^{2+}/CaM-dependent signaling process and the PKB cascade essential to the progression of apoptosis.

CaMKK is autoinhibited by a sequence located beyond the C-terminus of its catalytic domain (Fig. 1*a*)[14]. Site-directed mutagenesis identifies the regulatory domain of rat CaMKKα between residues 435 and 463. This comprises both autoinhibitory (residues 435–440) and CaM-binding (residues 438–463) regions, which are also conserved in a recently cloned β-isoform[15] and *Caenorhabditis elegans* CaMKK[16]. We have demonstrated that a synthetic peptide consisting of residues 438–463 is able to bind CaM in a Ca^{2+}-dependent manner, with a subnanomolar-range dissociation constant[17]. In addition, CaMKK is inactivated by protein kinase A (PKA) phosphorylating Ser 458, suggesting that phosphorylation may prevent Ca^{2+}/CaM from binding to the CaM-binding domain of CaMKK[18].

To date, the only known structures of Ca^{2+}/CaM–target complexes are those with peptides that specify the Ca^{2+}/CaM binding regions of myosin light chain kinase (MLCK)[19,20] and CaMKII[21]. All complexes reveal an α-helical target peptide clamped by the N- and C-terminal domains of CaM. A hydrophobic pocket in each CaM domain is deep enough to bind even the bulkiest residues (for example, Trp, Phe and Leu) of a target protein, and their sequential separation is often used to define particular binding modes. While not all separations will be possible, two distinct modes of binding are already known in the MLCK and CaMKII peptides, where the separations are 12 and 8 residues, respectively (Fig. 1*a*). The CaM-binding region of CaMKK appears to be a third distinct form. First, there are no candidate residues that could anchor the hydrophobic pocket in a manner similar to MLCKs and CaMKII (Fig. 1*a*). Second, a full binding activity of CaMKK for Ca^{2+}/CaM requires at least 26 residues, which is longer than both MLCKs and CaMKII. This suggests that Ca^{2+}/CaM binding to CaMKK must use a hitherto unobserved approach.

As a pivotal step toward clarifying this situation, we decided to determine the structure of Ca^{2+}/CaM bound to a synthetic peptide corresponding to the 26-residue region from α-isoform of rat CaMKK. We describe here the structure determination of the Ca^{2+}/CaM complex with the CaMKK peptide by NMR spectroscopy. The binding mode is entirely unanticipated, with the CaMKK peptide bound to the N- and C-terminal domains of CaM in the opposite orientation to all other known Ca^{2+}/CaM complexes as well as having deviations from the typically helical peptide conformation. Determinants for the peptide-binding orientation are also discussed.

Structure description

Our previous work using a series of C-terminal truncated mutants of rat CaMKKα has indicated that the region between residues 438 and 463 of CaMKKα was sufficient to bind to Ca^{2+}/CaM. Furthermore, site-directed mutagenesis studies have shown that mutations at 443–445, 448–450 or 455–457 significantly reduce Ca^{2+}/CaM binding activity[17]. In the present study, we have constructed two new mutants, F459D and F463D, both of which result in a total loss of CaM binding (Fig. 1*b*). Taking these data into consideration, we decided to use a peptide corresponding to residues 438–463 of rat CaMKKα for NMR structure determination .

The structure of Ca^{2+}/CaM complexed with the CaMKK peptide has been determined using 2,525 NOE-based distance restraints (including 271 intermolecular restraints), supplemented with 115 dihedral and 112 hydrogen bond restraints. The best-fit superposition of backbone atoms for 30 models, together with a ribbon diagram of the averaged structure, was generated (Fig. 1*c–e*). A summary of the structural statistics is given in Table 1.

The backbone conformation of N-terminal residues 1–75 (N-domain) and C-terminal residues 82–148 (C-domain) remains essentially unchanged upon binding to the CaMKK peptide. The

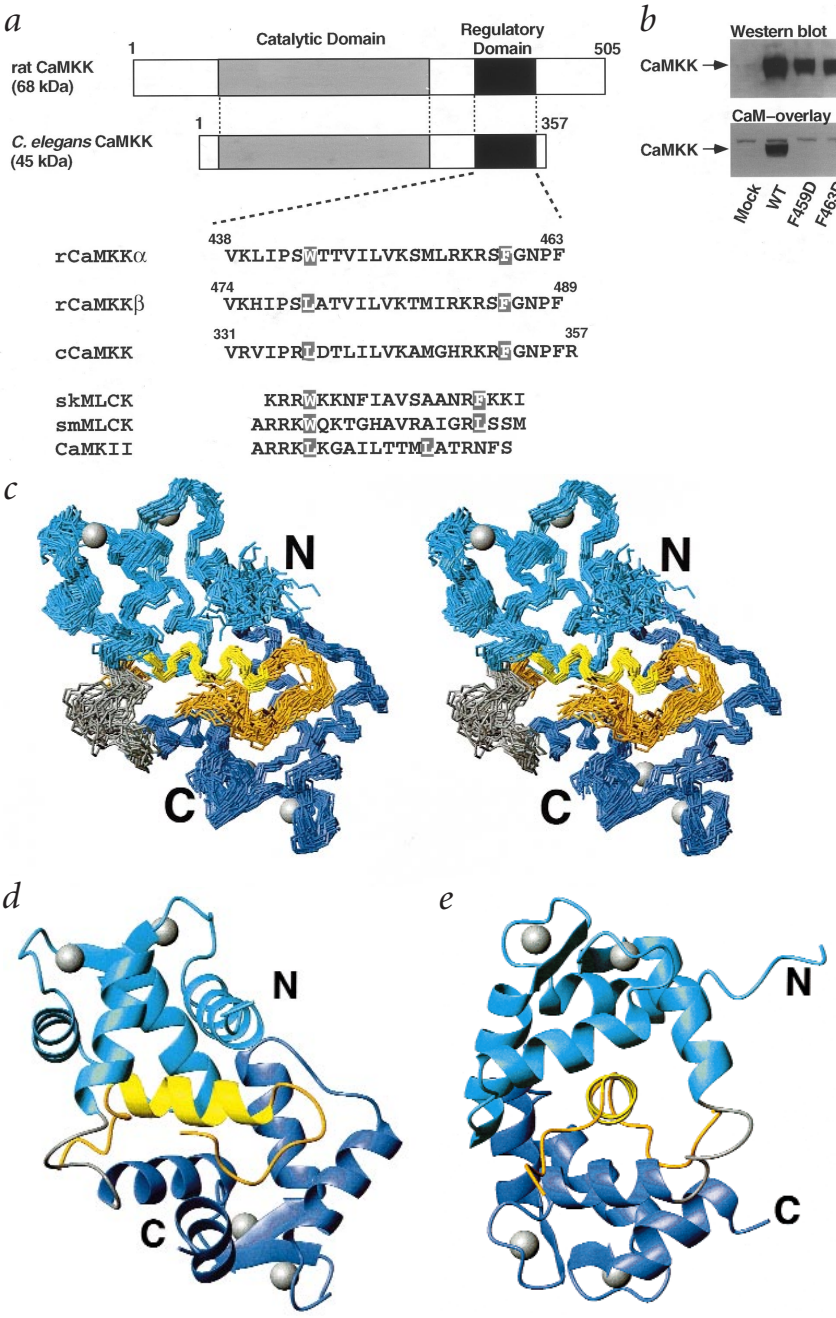

Fig. 1 ***a***, Alignment of Ca^{2+}/CaM binding sequences of CaMKK, MLCK and CaMKII. The key hydrophobic residues binding to the hydrophobic pockets of Ca^{2+}/CaM are shaded. The key residues of rat CaMKKβ and *C. elegans* CaMKK are proposed from this sequence alignment. Sequences: rCaMKKα, rat CaMKKα (residues 438–463)[17]; rCaMKKβ, rat CaMKKβ (residues 474–489)[15]; cCaMKK, *C. elegans* CaMKK (residues 331–357)[16]; skMLCK, rabbit skeletal muscle MLCK (residues 342–367)[19]; smMLCK, rabbit smooth muscle MLCK (residues 796–815)[20]; CaMKII, rat CaMKIIα (residues 290-315)[21]. ***b***, Binding of CaMKKα mutants (F459D and F463D) to Ca^{2+}/CaM. The binding of the mutants as well as wild type (WT) was analyzed by CaM overlay, and their expression was confirmed by western blotting. Mock, Extracts from mock-transfected COS-7 cells. ***c***, Stereo drawing of the 30 NMR models of the Ca^{2+}/CaM–CaMKK peptide complex. CaM N- and C-domains and the domain linker are shown in cyan, violet and gray, respectively. The helix and the loop region of the CaMKK peptide are shown in yellow and orange line, respectively. Ca^{2+} ions are shown as white spheres. Each model was superimposed onto the energy-minimized average structure using residues 6–18, 26–39, 45–55, 62–74, 83–91, 99–111, 118–127, 135–146 of Ca^{2+}/CaM and 443–463 of CaMKK. When using only backbone atoms (N, Cα and C), the r.m.s.d. was 0.78 ± 0.06 Å. For all heavy atoms (not shown), this increased to 1.38 ± 0.06 Å. ***d***, Front and ***e***, side view of the ribbon diagram of the energy-minimized averaged structure. The diagrams in (*c*–*e*) were generated using the program MOLMOL[55].

root-mean-square deviation (r.m.s.d.) values for the backbone atoms between Ca^{2+}/CaM[22] and the present structure are 0.96 Å for N-domain and 1.32 Å for C-domain. The larger r.m.s.d. value for C-domain is mainly due to a slight shift of helix VIII with respect to other helices in C-domain; interhelical angles between helix V and VIII and between helix VI and VIII undergo greater changes (-15.0 ± 4.6° and 22.2 ± 4.1°, respectively) compared with those between all other helix pairs (<8.0°). A drastic change in the overall CaM conformation upon binding to the CaMKK peptide occurs at the domain linker region. When CaM is free from a target, the domain linker displays high flexibility at residues 78–81 in solution[23]. Upon binding to the CaMKK peptide, this portion in the linker undergoes further melting, resulting in a longer flexible loop comprising residues 75–82. This change in the linker region enables the two domains to come together and clamp the CaMKK peptide effectively (Fig. 1*c*–*e*). Similar methods in recognizing target proteins have been observed in CaM–MLCK[19,20] and CaM–CaMKII[21] complexes.

However, it is here that overall resemblance to other CaM–peptide complexes ends. Unlike the previously determined CaM-bound target peptides that form an α-helix upon complexation, the CaMKK peptide consists of two structural segments (Fig. 2*a*): an 11-residue α-helix (residues 444–454) connected to a hairpin-like loop (residues 455–459) whose C-terminus folds back onto the helix. Both the α-helix and the hairpin-like loop are involved in interactions with CaM. Extensive hydrophobic contacts involving a number of side chains between the peptide and CaM were observed in $^{13}C/F_3$-filtered $^{13}C/F_1$-edited HMQC-NOESY[24] spectrum. The N-terminal portion of the peptide helix employs Trp 444 to interact with many CaM residues including Ile 27 and Ile 63 (Fig. 2*b*). This tryptophan residue serves as a key hydrophobic residue that anchors to CaM N-domain (Fig. 2*c*). The C-terminal portion of the helix and the hairpin loop mainly interact with the hydrophobic pocket of CaM C-domain. This hairpin loop provides Phe 459, another key hydrophobic residue interacting with Val 91, Leu 112 and Val 136 of C-domain (Fig. 2*b*,*d*). The interaction of residues following Phe 459 with helix VIII of C-domain, is probably responsible for the slight shift of the helix VIII described above. In addition, the loop is stabilized by intramolecular hydrophobic interactions between Met 453 and Phe 459, as

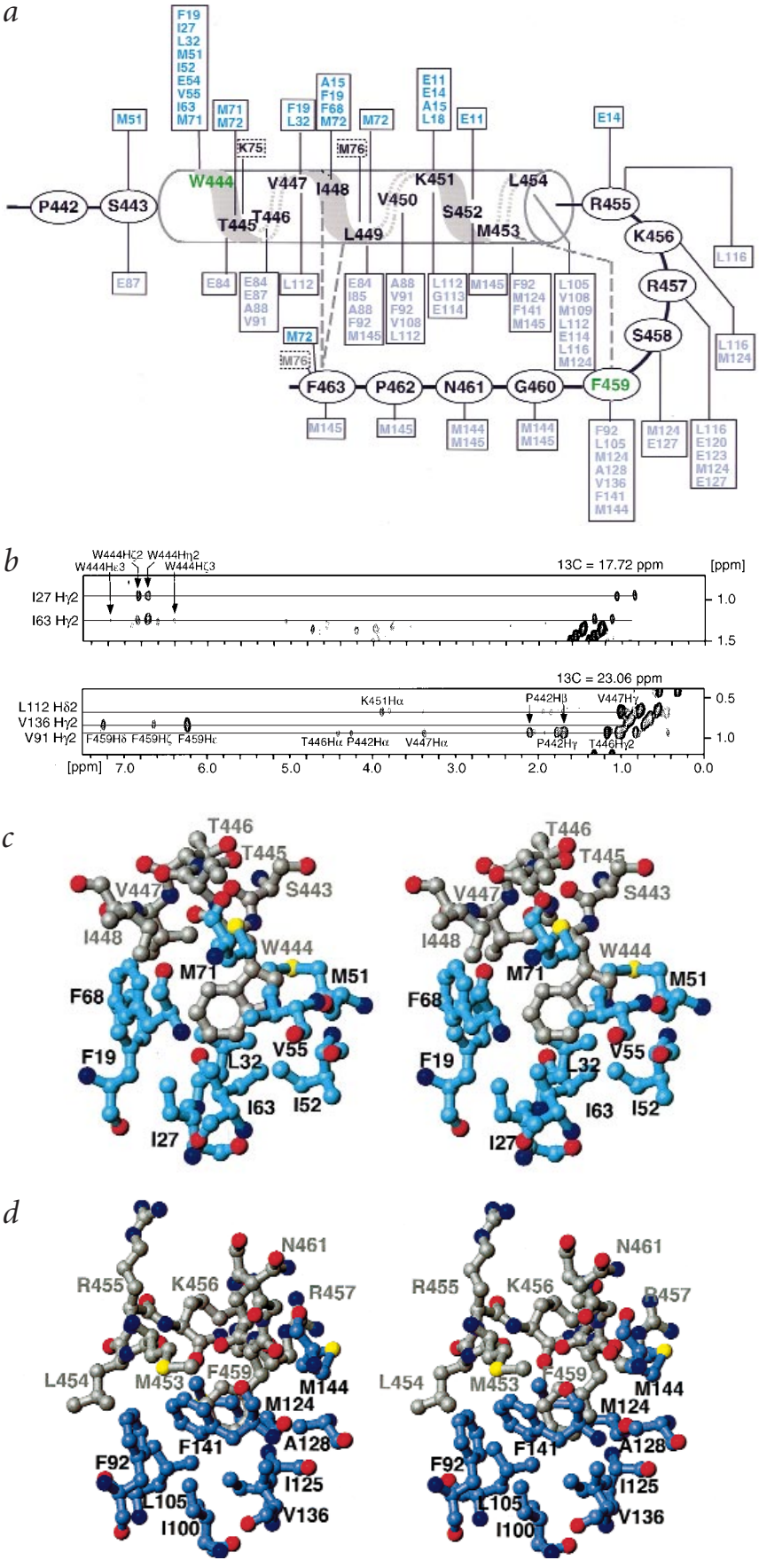

Fig. 2 ***a***, Schematic drawing of interacting residues between Ca^{2+}/CaM and CaMKK peptide. Residues in N-domain and C-domain are colored in cyan and violet, respectively. Key residues of the CaMKK peptide anchoring the hydrophobic pocket in each domain, Trp 444 and Phe 459, are shown in green. ***b***, Portions of $^{13}C/F_3$-filtered $^{13}C/F_1$-edited HMQC-NOESY spectrum[24] showing intermolecular NOEs between CaM and the CaMKK peptide. Stereo drawing of the key residues of CaMKK peptide in the hydrophobic pocket of ***c***, N-domain and ***d***, C-domain. Residues within 5 Å of the key residues, Trp 444 and Phe 459, are shown. N, O and S atoms are colored in blue, red and yellow, respectively, while C atoms of N- and C-domain of CaM and CaMKK are shown in cyan, violet and gray, respectively. Diagrams (*c*) and (*d*) were generated using the program MOLMOL[55].

well as interactions involving Phe 463, Ile 448 and Leu 449. The final residue of our peptide, Phe 463, also makes intimate contact with Met 72 and Met 76 of CaM.

Interactions between three basic residues (Arg 455, Lys 456 and Arg 457) of the loop structure and the negatively charged CaM residues, Glu 14, Glu 120, Glu 123 and Glu 127 (Fig. 2*a*), probably contribute intermolecular electrostatic interactions. Interestingly, phosphorylation of Ser 458 by PKA has been shown to abolish the CaMKK activity[18]. In the present structure, this serine is located in the vicinity of Glu 127 of CaM. Phosphorylation of Ser 458 would introduce a negative charge to this local environment, possibly repelling the glutamic acid. However, given the relatively large binding surface of the peptide–protein complex (3,410 Å^2), it is not yet clear why this single modification is sufficient to modulate CaMKK activity so drastically.

Correlation with mutagenesis studies

Our structure of the CaM–CaMKK peptide complex is consistent with previous mutagenesis studies on CaMKK, in which block aspartate scanning was used to mutate four nonoverlapping blocks[17]. Of the four block mutants, those involving residues 443–445, 448–450 and 455–457 showed no binding affinity for Ca^{2+}/CaM and suppressed CaMKK enzymatic activity by about 80% under the experimental conditions used. Residues 443–445 and 448–450 correspond to the helix, whereas residues 455–457 are in the hairpin loop of our present structure; all of these are crucial for the interaction with CaM. The mutant with the fourth block, involving residues 438–440, showed about 80% reduction in Ca^{2+}/CaM binding activity. This region is just N-terminal of the CaM-binding core of the peptide in our struc-

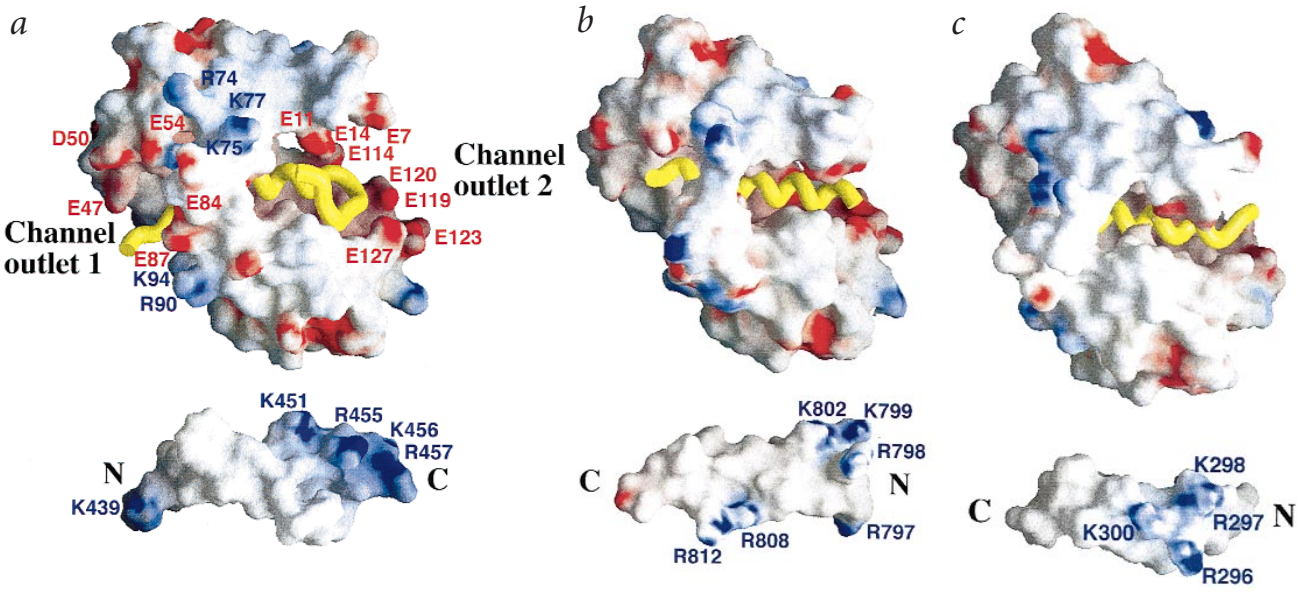

Fig. 3 Electrostatic potential surfaces of the CaM–target peptide complexes. In the upper panels, the surface of Ca^{2+}/CaM is shown with the target peptide as an yellow tube. The peptide surface is in the lower panels. The surface is colored according to the local electrostatic potential, with blue and red representing positive and negative potential, respectively. Acidic and basic residues interacting with the target peptide are labeled in red and blue, respectively. ***a***, CaM–CaMKK; ***b***, CaM–MLCK[19,20]; ***c***, CaM–CaMKII[21]. The domain linker of CaM in the CaM–CaMKII complex was modeled in the Insight II, since residues 74–83 are absent from the PDB file because of the high flexibility of this region. This figure was generated using GRASP[56]

ture. The simultaneous replacement of the three residues with aspartates probably caused intermolecular electrostatic repulsions, since there are many acidic residues in the region of CaM, which binds the N-terminus of the CaMKK peptide (see later).

Furthermore, point mutations at two single sites in the hairpin loop (F459D and F463D) resulted in total loss of Ca^{2+}/CaM affinity under the same condition used for the block aspartate scanning (Fig. 1*b*). In the present structure, the complex is clearly stabilized by these residues located in the hairpin loop, providing hydrophobic interactions with C-domain as well as residues in its own CaMKK helix. A recent mutagenesis study[25] indicated that a truncated mutant of $CaMKK_{1–457}$ retains Ca^{2+}/CaM sensitivity in the phosphorylation activity. This is not surprising, since most residues (16 out of 22) essential for CaM–CaMKK interaction (Fig. 2*a*) remain in the mutant. However, lack of residues 458–463 may account for the reduction in Ca^{2+}/CaM-dependent enzyme activation[25]. This notion is supported by our mutagenesis studies in which the ability to bind to CaM is undetectable for the F463D mutant (Fig. 1*b*).

Comparison with other CaM–peptide complexes

The most striking feature of this structure concerns the orientation of the peptide with respect to the N- and C-domains of CaM. In all previously known cases (that is, CaM–skeletal muscle MLCK peptide[19], CaM–smooth muscle MLCK[20], CaM–CaMKII[21]), the peptide helix is positioned such that the N-terminal portion mainly binds to C-domain of CaM, while the C-terminal portion binds to CaM N-domain (Fig. 3*b,c*). To our surprise, the peptide orientation in the CaM–CaMKK complex is reversed (Fig. 3*a*); the N-terminal portion of the CaMKK peptide interacts with N-domain, while the C-terminal portion of the peptide binds to C-domain.

Another key feature of the structure is the position of the two key hydrophobic residues that anchor the peptide to CaM N- and C-domains. In both skeletal and smooth muscle MLCK peptides, there are 12 residues between the two key anchoring residues, whereas in CaM–CaMKII there are eight. In the present structure of the CaM–CaMKK peptide complex, the spacer between Trp 444 and Phe 459 comprises 14 residues, representing the longest among those so far characterized. Consistent with the lengths of the spacer among different complexes, the structure of the CaM–CaMKK complex is closer to that of the CaM–MLCK complex than to that of the CaM–CaMKII complex. More quantitatively, the r.m.s.d. value for the CaM backbone atoms of residues 11–73 and 84–146 between CaMKK and MLCK complexes (1.75 Å) is smaller than the corresponding value of CaMKK and CaMKII (2.54 Å). As previously noted by various groups[23,26–28], the high flexibility of the domain linker in CaM is clearly important in allowing CaM to adopt various binding configurations.

Determinants for the peptide-binding direction

Close examination of the present structure together with the previously published CaM–peptide complexes[19–21] identifies two important features of the target-binding channel formed by N- and C-domains of CaM (Fig. 3). The first feature is electrostatic polarity of the channel created by a non-uniform distribution of acidic and basic residues at the two channel outlets (Fig. 3*a*). Channel outlet 1 (CO-1) possesses seven acidic residues and four basic residues, whereas channel outlet 2 (CO-2) contains eight acidic residues but no basic residue. As a result, CO-2 is more negatively charged than CO-1. In particular, Lys 75, Arg 86 and Arg 90 contribute largely to neutralization of acidic clusters of the CO-1. This feature is common in all structures of CaM–peptide complexes that have been solved (Fig. 3*b,c*).

The second feature involves the domain linker location relative to the two channel outlets of CaM. CO-1 is created by helices II, III and IV from N-domain and helix V of C-domain, whereas CO-2 results from helix I from N-domain and helices

Fig. 4 Alignment of the sequences of CaM-binding region based on the position of the N-terminal key residue. The peptides whose structure in complex with Ca^{2+}/CaM has been determined are underlined. Key residues are shaded. Acidic and basic residues are shown in red and blue, respectively. Sequences for MLCK, rat CaMKII (rCaMKII) and CaMKK peptides are the same as in Fig. 1*a*. Other sequences were taken from the reference of Rhoads and Friedberg[57]: CaMKI, rat CaMKI (residues 300–317)[29]; mouse CaMKIV (residues 319–338)[30]; *Neurospora crassa* calcineurin (residues 406–425)[31]; *Drosophila* myosin ninaC (residues 1040–1059)[32]; rat guanine nucleotide-releasing protein (GNRP, residues 206–225)[33]. On the right are schematically depicted observed or predicted binding polarity of these sequences.

VI, VII and VIII of C-domain. Importantly, the domain linker, which resides between helix IV and V, partially covers CO-1 (Fig. 3*a*), resulting in CO-1 being smaller than CO-2.

Not surprisingly, the target peptides possess complementary properties. Specific steric and electrostatic effects define a clear binding mode for CaMKK. The hairpin loop makes the C-terminal portion of CaMKK peptide bulkier than the N-terminal portion, such that the C-terminus would only fit CO-2. Electrostatic polarity is also a prominent determinant (Fig. 3*a*), with the CaMKK peptide possessing a C-terminal postively charged cluster that interacts with CO-2. In the MLCK and CaMKII peptides, a similar basic cluster at the N-terminus interacts with CO-2 (Fig. 3 *b,c*). Being slightly bulkier, the basic cluster provides an additional steric preference, which is consistent with the structure of the Ca^{2+}/CaM–CaMKK peptide complex.

Based on these particular characteristics, one can predict the binding orientation of a given target protein with CaM domains. For example, CaM-dependent kinases I (ref. 29) and IV (ref. 30), and calcineurin[31] share the same properties as MLCK and CaMKII (Fig. 4); a basic cluster located at the N-terminal portion of the CaM-binding domain. Therefore, these enzymes are likely to bind to CaM in a similar orientation as the CaM–MLCK and –CaMKII complexes. On the other hand, *C. elegans* CaMKK, *Drosophila* unconventional myosin[32], and rat guanine nucleotide-releasing protein[33] possess a basic cluster at their C-termini. So these proteins will probably bind to CaM, in a manner similar to the present structure. However, this still leaves a few cases in which a basic cluster is not apparent, such as the human Ca^{2+} pump[34] and plant glutamate decarboxylase[35].

Table 1 Statistics of the 30 structures of Ca^{2+}/CaM complexed with CaMKK peptide[1]

R.m.s. deviations from experimental distance restraints (Å)	
All (2,383/278 with 271 intermolecular NOEs)	0.0177 ± 0.0004
Interresidue sequential NOE (|i - j| = 1) (468/65)	0.022 ± 0.003
Interresidue short-range NOE (1 < |i - j| ≤ 5) (337/29)	0.020 ± 0.012
Interresidue long-range NOE (|i - j| > 5) (362/20)	0.008 ± 0.003
Intraresidue NOE (823/150)	0.014 ± 0.005
Intermolecular NOE (271)	0.023 ± 0.002
Hydrogen bond (98/14)	0.022 ± 0.002
R.m.s. deviations from experimental dihedral restraints (°) (105/10)	0.07 ± 0.04
R.m.s. deviations from idealized geometry	
Bonds (Å)	0.0028 ± 0.0002
Angles (°)	0.485 ± 0.006
Impropers (°)	0.358 ± 0.003
Energies (kcal mol^{-1})	
F_{NOE}[2]	41.9 ± 6.3
F_{cdih}[2]	0.09 ± 0.12
F_{repel}[3]	9.2 ± 2.5
F_{L-J}[4]	-317.6 ± 48.3
R.m.s. deviations from the mean structure (Å)	
Backbone heavy atoms (superimposed on N, Cα, C)	0.78 ± 0.06
All heavy atoms	1.38 ± 0.06

[1]The number of each type of restraints used in the structure calculation is given in parentheses. None of the structures exhibits distance violations greater than 0.3 Å or dihedral angle violations greater than 1.0°.
[2]F_{NOE} and F_{cdih} were calculated using force constraints of 50 kcal mol^{-1} $Å^{-2}$ and 200 kcal mol^{-1} rad^{-2}, respectively.
[3]F_{repel} was calculated using a final value of 4.0 kcal mol^{-1} $Å^{-4}$ with the van der Waals hard sphere radii set to 0.75 times those in the parameter set PARALLHSA supplied with X-PLOR[54].
[4]F_{L-J} is the Lennard–Jones van der Waals energy calculated with the CHARMM empirical energy function and is not included in the target function for simulated-annealing calculation.
[5]Each model was superimposed onto the energy-minimized average structure using residues 6–18, 26–39, 45–55, 62–74, 83–91, 99–111, 118–127, 135–146 of Ca^{2+}/CaM and 443–463 of CaMKK.

Concluding remarks

The present structure reveals that CaMKK uses a unique CaM-binding mechanism that differs from those observed for MLCKs[19,20] and CaMKII[21]. While the MLCK and CaMKII peptides adopt α-helical conformations in the CaM-binding region, the CaMKK peptide assumes a fold comprising a helix and a hairpin-like loop, both of which are essential for CaM binding. Orientation of the CaMKK peptide with respect to the two CaM domains is opposite to that of the MLCK and CaMKII peptides. We suggest that electrostatic attraction at the channel outlets formed by the two CaM domains play a key role in determining the binding orientation of the target protein. The location of the domain linker with respect to the channel outlets may also induce larger steric hindrance at one channel compared to the other. These features appear to represent critical determinants for CaM binding to its target proteins.

Methods

Sample preparation. A 26-residue synthetic peptide corresponding to the calmodulin-

binding domain of rat CaMKKα was synthesized by Peptide Institute Inc. Uniformly ^{15}N- or ^{13}C/^{15}N-labeled recombinant *Xenopus laevis* CaM was expressed in *Escherichia coli* and purified to homogeneity as described[36]. CaM was dissolved in unbuffered 0.4 ml 95% H_2O/5% D_2O or 99.99% D_2O v/v solution containing 0.1 M KCl and 10 mM $CaCl_2$. The pH/pD values of the samples were 6.7 without consideration of the isotope effects. The sample concentrations of CaM were 1.5 mM. The molar ratio of CaM and the CaMKK peptide was 1:1.25 for the sample used for the structure determination to ensure complete formation of the complex.

NMR spectroscopy. All NMR experiments were performed at 30 ºC on a Bruker AMX-600 spectrometer. Sequential assignments of the backbone resonances of CaM were achieved by the sets of experiments, HNCACB[37] and CBCA(CO)NH[38,39], CT-HNCO[40], gd-HCACO[41], ^{15}N-edited TOCSY-HMQC, HNHA[42] and HBHA(CBCACO)NH[43]. Side chain assignments were obtained from H(CCO)NH[44], C(CO)NH[44] and HCCH-TOCSY[45] experiments. Stereospecific assignments of valine and leucine methyl groups were obtained by analyzing a constant-time ^{13}C-^{1}H HSQC spectrum of 10% ^{13}C-enriched Ca^{2+}/CaM complexed with CaMKK peptide[46].

The assignments of the CaMKK peptide were carried out based on NOE connectivities by analyzing a series of isotope filter experiments[47]: ^{15}N/F_2-filtered NOESY and TOCSY, ^{13}C,^{15}N/F_2-filtered NOESY and TOCSY, ^{13}C/F_1,F_2-filtered NOESY, TOCSY and COSY. All data were processed using the software NMRPipe[48], and the data analysis was assisted by the software PIPP[49].

The ^{1}H, ^{13}C and ^{15}N resonance assignments have been deposited with the BioMagResBank, with accession number 4270.

Structure calculation. Approximate interproton distances were obtained from ^{13}C-edited NOESY-HMQC[50], ^{15}N-edited NOESY-HMQC[51], ^{13}C/F_3-filtered ^{13}C/F_1-edited HMQC-NOESY[24], and isotope-filtered NOESY spectra described above. The mixing time was 100 ms for all NOESY experiments. The distance restraints were grouped into four classes: 1.8–2.7 Å, 1.8–3.3 Å, 1.8–5.0 Å and 1.8–6.0 Å corresponding to strong, medium, weak and very weak NOE cross peak intensities, respectively. The NOEs including backbone amide protons were grouped into four classes of 1.8–2.9 Å, 1.8–3.5 Å, 1.8–5.0 Å and 1.8–6.0 Å. The backbone coupling constants, $^{3}J_{NH\alpha}$, were measured from a HNHA experiment[42]. ϕ- and ψ-dihedral angle restraints were derived from the $^{3}J_{NH\alpha}$ coupling constants and chemical shift indices[52]. Values of -60° ± 30° and -40° ± 30° were used for ϕ- and ψ-dihedral angles, respectively, for α-helical regions; -120° ± 50° and 120° ± 50° for β-strands. Hydrogen bond restraints were obtained by analyzing the H/D exchange rates and the NOE patterns characteristic of α-helices or β-strands. Two distance restraints, r_{NH-O}(0–2.3 Å) and r_{N-O}(0–3.3 Å), were used for each hydrogen bond. Structures were calculated using the YASAP protocol[53] within X-PLOR 3.1 (ref. 54).

Mutagenesis and transient expression of CaMKK mutants. Rat CaMKKα cDNA (GenBank accession number L42810) was from a rat brain cDNA library[5]. Mutagenesis of CaMKK (F459D and F463D) using pME-CaMKK (wild type) plasmid as a template was carried out by GeneEditor *in vitro* Site-Directed Mutagenesis System (Promega Co.). Transient expression of CaMKK mutants (F459D, F463D) was carried out as described[17]. Extracts from COS-7 cells (18 μg) that were either mock-transfected or transfected with the indicated rat CaMKKα mutants (F459D, F463D) including wild type, were subjected to 10% SDS-PAGE and transferred onto Immobilon C (Millipore Corp.). Membranes were analyzed by western blotting using anti CaMKK antibody (Transduction Lab.) and CaM overlay.

Coordinates. The coordinates for the final structures and structural constraints used in the calculations have been deposited with the Protein Data Bank (accession code 1CKK).

Acknowledgments

We are grateful to C. Klee for kindly providing the *Xenopus* calmodulin expression system, K.I. Tong for calmodulin purification, N. Takahashi for the mutagenesis experiments, R. Ishima and T. Tanaka for NMR experiments and discussions. This work was in part supported by a grant (to M.I.) from Medical Research Council of Canada (MRCC). M.I. is a Howard Hughes Medical Institute International Research Scholar and MRCC Scientist.

Correspondence should be addressed to M.I. *email: mikura@oci.utoronto.ca*

Received 3 May, 1999; accepted 22 June, 1999.

1. Tokumitsu, H. *et al. J. Biol. Chem.* **269**, 28640–28647 (1994).
2. Okuno, S. & Fujisawa, H. *J. Biochem. (Tokyo)* **114**, 167–170 (1993).
3. Okuno, S., Kitani, T. & Fujisawa, H. *J. Biochem. (Tokyo)* **116**, 923–930 (1994).
4. Lee, J.C. & Edelman, A.M. *J. Biol. Chem.* **269**, 2158–2164 (1994).
5. Tokumitsu, H., Enslen, H. & Soderling, T.R. *J. Biol. Chem.* **270**, 19320–19324 (1995).
6. Bading, H., Ginty, D.D. & Greenberg, M.E. *Science* **260**, 181–186 (1993).
7. Enslen, H., *et al. J. Biol. Chem.* **269**, 15520–15527 (1994).
8. Sun, P., Enslen, H., Myung, P.S. & Maurer, R.A. *Genes Dev.* **8**, 2527–2539 (1994).
9. Matthews, R.P. *et al. Mol. Cell. Biol.* **14**, 6107–6116 (1994).
10. Enslen, H., Tokumitsu, H. & Soderling, T.R. *Biochem. Biophys. Res. Commun.* **207**, 1038–1043 (1995).
11. Bito, H., Deisseroth, K. & Tsien, R.W. *Cell* **87**, 1203–1214 (1996).
12. Bito, H., Deisseroth, K. & Tsien, R.W. *Curr. Opin. Neurobiol.* **7**, 419–429 (1997).
13. Yano, S., Tokumitsu, H. & Soderling, T.R. *Nature* **396**, 584–587 (1998).
14. Tokumitsu, H. & Soderling, T.R. *J. Biol. Chem.* **271**, 5617–5622 (1996).
15. Kitani, T., Okuno, S. & Fujisawa, H. *J. Biochem. (Tokyo)* **122**, 243–250 (1997).
16. Tokumitsu, H., Takahashi, N., Yano, S., Soderling, T.R. & Muramatsu, M. *J. Biol. Chem.* **274** 15803–15810 (1999).
17. Tokumitsu, H., Wayman, G.A., Muramatsu, M. & Soderling, T.R. *Biochemistry* **36**, 12823–12827 (1997).
18. Wayman, G.A., Tokumitsu, H. & Soderling, T.R. *J. Biol. Chem.* **272**, 16073–16076 (1997).
19. Ikura, M. *et al. Science* **256**, 632–638 (1992).
20. Meador, W.E., Means, A.R. & Quiocho, F.A. *Science* **257**, 1251–1255 (1992).
21. Meador, W.E., Means, A.R. & Quiocho, F.A. *Science* **262**, 1718–1721 (1993).
22. Babu Y.S., Bugg, C.E. & Cook, W.J. *J. Mol. Biol.* **204**,191–204.
23. Barbato, G., Ikura, M., Kay, L.E., Pastor, R.W. & Bax, A. *Biochemistry* **31**, 5269–5278 (1992).
24. Lee, W., Revington, M.J., Arrowsmith, C. & Kay, L.E. *FEBS Lett.* **350**, 87–90 (1994).
25. Matsushita, M. & Nairn, A.C. *J. Biol. Chem.* **273**, 21473–21481 (1998).
26. Ikura, M., *et al. Biochemistry* **30**, 9216–9228 (1991).
27. van der Spoel, D., de Groot, B.L., Hayward, S., Berendsen, H.J. & Vogel, H.J. *Protein Sci.* **5**, 2044–2053 (1996).
28. Persechini, A. & Kretsinger, R.H. *J. Biol. Chem.* **263**, 12175–12178 (1988).
29. Picciotto, M.R., Czernik, A.J. & Nairn, A.C. *J. Biol. Chem.* **268**, 26512–26521 (1993).
30. Jones, D.A., Glod, J., Wilson-Shaw, D., Hahn, W.E. & Sikela, J.M. *FEBS Lett.* **289**, 105–109 (1991).
31. Higuchi, S., Tamura, J., Giri, P.R., Polli, J.W. & Kincaid, R.L. *J. Biol. Chem.* **266**, 18104–18112 (1991).
32. Montell, C. & Rubin, G.M. *Cell* **52**, 757–772 (1988).
33. Shou, C., Farnsworth, C.L., Neel, B.G. & Feig, L.A. *Nature* **358**, 351–354 (1992).
34. Verma, A.K. *et al. J. Biol. Chem.* **263**, 14152–14159 (1988).
35. Yuan, T. & Vogel, H.J. *J. Biol. Chem.* **273**, 30328–30335 (1998).
36. Ikura, M., Kay, L.E. & Bax, A. *Biochemistry* **29**, 4659–4667 (1990).
37. Wittekind, M. & Mueller, L. *J. Magn. Reson.* **B101**, 201–205 (1993).
38. Grzesiek, S. & Bax, A. *J. Am. Chem. Soc.* **114**, 6291–6293 (1992).
39. Szyperski, T., Pellecchia, M. & Wüthrich, K. *J. Magn. Reson.* **B105**, 188–191 (1994).
40. Grzesiek, S. & Bax, A. *J. Magn. Reson.* **96**, 432–440 (1992).
41. Zhang, W. & Gmeiner, H. *J. Biomol. NMR* **7**, 247–250 (1996).
42. Vuister, G.W. & Bax, A. *J. Am. Chem. Soc.* **115**, 7772–7777 (1993).
43. Grzesiek, S. & Bax, A. *J. Biomol. NMR* **3**, 185–204 (1993).
44. Grzesiek, S., Anglister, J. & Bax, A. *J. Magn. Reson.* **B101**, 114–119 (1993).
45. Bax, A., Clore, G.M. & Gronenborn, A.M. *J. Magn. Reson.* **88**, 425–431 (1990).
46. Neri, D., Szyperski, T., Otting, G., Senn, H. & Wüthrich, K. *Biochemistry* **28**, 7510–7516 (1989).
47. Ikura, M. & Bax, A. *J. Am. Chem. Soc.* **114**, 2433–2440 (1992).
48. Delaglio, F. *et al. J. Biomol. NMR* **6**, 277–293 (1995).
49. Garrett, D.S., Powers, R., Gronenborn, A.M. & Clore, G.M. *J. Magn. Reson.* **95**, 214–220 (1991).
50. Ikura, M., Kay, L.E., Tschudin, R. & Bax, A. *J. Magn. Reson.* **86**, 204–209 (1990).
51. Marion, D., Kay, L.E., Sparks, S.W., Torchia, D.A. & Bax, A. *J. Am. Chem. Soc.* **111**, 1515–1517 (1989).
52. Wishart, D.S. & Sykes, B.D. *Methods Enzymol.* **239**, 363–392 (1994).
53. Nilges, M., Gronenborn, A.M., Brünger, A.T. & Clore, G.M. *Protein Eng.* **2**, 27–38 (1988).
54. Brünger, A.T. X–PLOR Version 3.1. A system for X-ray crystallography and NMR (Yale University Press, New Haven; 1992).
55. Koradi, R., Billeter, M., & Wüthrich, K. *J. Mol. Graphics* **14**, 51–55 (1996).
56. Nicholls, A., Sharp, K.A. & Honig, B. *Proteins* **11**, 281–293 (1991).
57. Rhoads, A.R. & Friedberg, F. *FASEB J.* **11**, 331–340 (1997).